Journal of Power Sources 268 (2014) 146–152

Contents lists available at ScienceDirect

Journal of Power Sources

journal homepage: www.elsevier.com/locate/jpowsour

Short communication

Novel efficient synthesis of nanosized carbon coated $LiMnPO_4$ composite for lithium ion batteries and its electrochemical performance

Jianguo Duan, Yanbing Cao*, Jianbing Jiang, Ke Du, Zhongdong Peng, Guorong Hu

School of Metallurgy and Environment, Central South University, Changsha 410083, PR China

HIGHLIGHTS

- A novel eco-efficient $LiMnPO_4$ synthesis process was developed by involving mechano-chemical reaction between Mn and LiH_2PO_4.
- In situ carbon coated $LiMnPO_4$/C composites with a 20 ~ 50 nm particle size distribution was successfully obtained.
- LiMnPO4/C samples with reduced carbon amount displays excellent electrochemical performance.

GRAPHICAL ABSTRACT

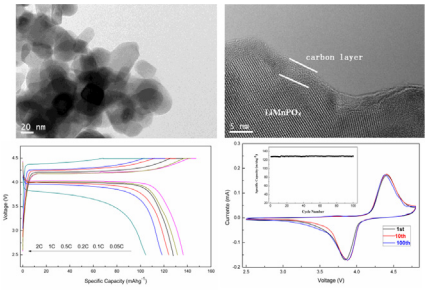

ARTICLE INFO

Article history:
Received 26 March 2014
Received in revised form
16 May 2014
Accepted 3 June 2014
Available online 11 June 2014

Keywords:
Composite materials
Mechano-chemical liquid-phase activation
Electron microscopy
Electrochemical properties

ABSTRACT

An eco-efficient approach bases on a mechano-chemical liquid-phase activation technique is developed for synthesizing $LiMnPO_4$/C composites. The fine sized $[Mn_3(PO_4)_2{\cdot}xH_2O + Li_3PO_4]$ precursors with uniform particle size distribution are prepared, and characterized by XRD and scanning electron microscope (SEM). The in—situ carbon coated $LiMnPO_4$ composites are synthesized by one-step solid state reaction. The prepared $LiMnPO_4$/C nano-composites show a comparable rate capability with discharge specific capacity of 136.4 mAh g^{-1} at 0.05 C-rate and 118 mAh g^{-1} at 1 C-rate at room temperature. The results indicate that $LiMnPO_4$/C composites synthesize from this environmental friendly route shows a promising electrochemical activity as cathode material for lithium ion batteries.

1. Introduction

Currently, the interest in Li-ion batteries is driven by its dominating of the market for portable electronics and expanding its application for the electricity powered transportation [1]. A strong research effort has been focused on developing new cathode materials to improve its energy density, safety, stability as well as cost-effectiveness [2]. Among the cathode members, $LiMnPO_4$ becomes a most promising material in the family of olivine phosphate since its high reversible capacity (170 mAh g^{-1}), high energy density (697 Wh Kg^{-1}) and good chemical & thermal stability [3]. However, the high ionic and electronic resistance of $LiMnPO_4$ has rendered it difficult to obtain highly electrochemical activity [4–9]. The above negative aspects can however be compensated by reducing structure size and coating suitable conductive layers [10,11].

To achieve the desired composite architecture, one needs to focus on the material synthesis since the particle size, the degree of particle agglomeration as well as the local distribution of conductive phase are difficult to regulate once the composite material has

* Corresponding author. Tel.: +86 13875868540.
E-mail addresses: cybcsu@csu.edu.cn, csudjg@163.com (Y. Cao).

http://dx.doi.org/10.1016/j.jpowsour.2014.06.020
0378-7753/

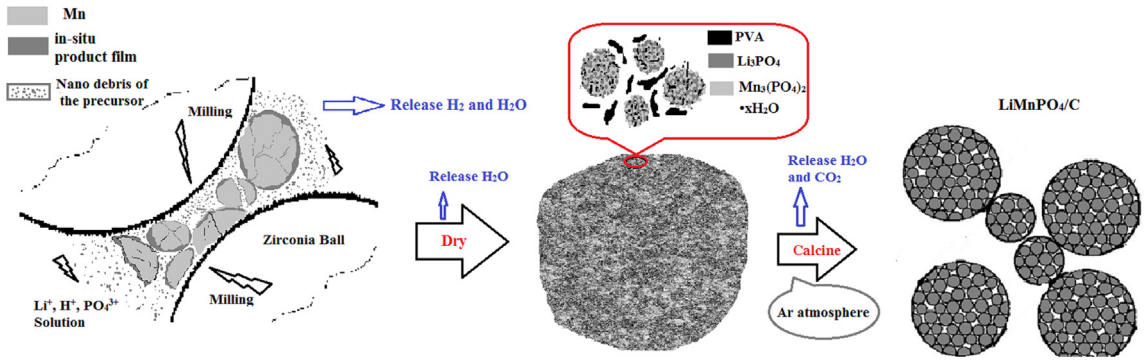

Fig. 1. Schematic presentation of the mechanical liquid activation heterogeneous reaction synthesis process.

been synthesized. In this context, successful syntheses of excellent cathodes have been performed using precipitation route [5,11–20], hydrothermal route [21–28] and polyol method [9,29]. However, most of these synthetic processes suffer from the problems of complex manufacturing processes, expensive raw materials, low atom utilization, and waste solution treatment. Therefore, it is of practical importance to develop simple and eco-efficient synthesis for $LiMnPO_4$ with optimization of morphology and structure in large volume.

From the simplicity and environmental points of view, a heterogeneous reaction in liquid phase medial at room temperature using low-cost reagents has been proposed for nano-$LiMnPO_4$ synthesis by keeping bunk production in mind. Here, a modified solid–liquid reaction process was developed involving mechanochemical activation between Mn and LiH_2PO_4, with the addition of PVA (Polyvinyl alcohol) as carbon source for synthesis $LiMnPO_4$/C nano-composites. In this typical process, the change of the structure of solid particles in the mechanochemical process results in the heterogeneous reaction smoothly between Mn and LiH_2PO_4 without filtration/washing step during the whole synthesis processing. Moreover, from the materials processing point of view, only H_2, CO_2 and H_2O are released from the whole synthesis process, this mechanical liquid-phase activation process is a cost-effective and facile route to manufacture high performance $LiMnPO_4$ materials in large scales.

2. Experimental

In a typical process, stoichiometric amount of Mn powder (99.34% + pure), LiH_2PO_4 (99.7% + pure) and PVA (99% + pure, GJ29-JX09, the length (n) is 2400 ~ 2500, 5 g PVA/0.1 mol Mn) were milled in a liquid environment. A planetary ball mill with tow cylindrical zirconia vials having the capacity of 250 ml each was employed for powder milling. The mixture was ball milled thoroughly with zirconia balls (ball-to-powder weight ration 20 to 1) at room temperature for 6 h at 400 rpm. The slurry then dried at 55 °C for 12 h.

In order to prepare $LiMnPO_4$/C, the mixture was then calcined at 650 °C for 4 h in Ar atmosphere with a heating rate of 3 °C min^{-1}. After cooling in furnace, the final black powders ($LiMnPO_4$/C) were obtained. The schematic presentation of the synthesis procedure is shown in Fig. 1.

The thermal behavior of the mixture was investigated by thermogravimetric analysis (TGA/DSC, NETZSCH STA 449C). The TGA/DSC experiments were carried out in Ar atmosphere from 30 to 800 °C with a heating rate of 10 °C min^{-1}.

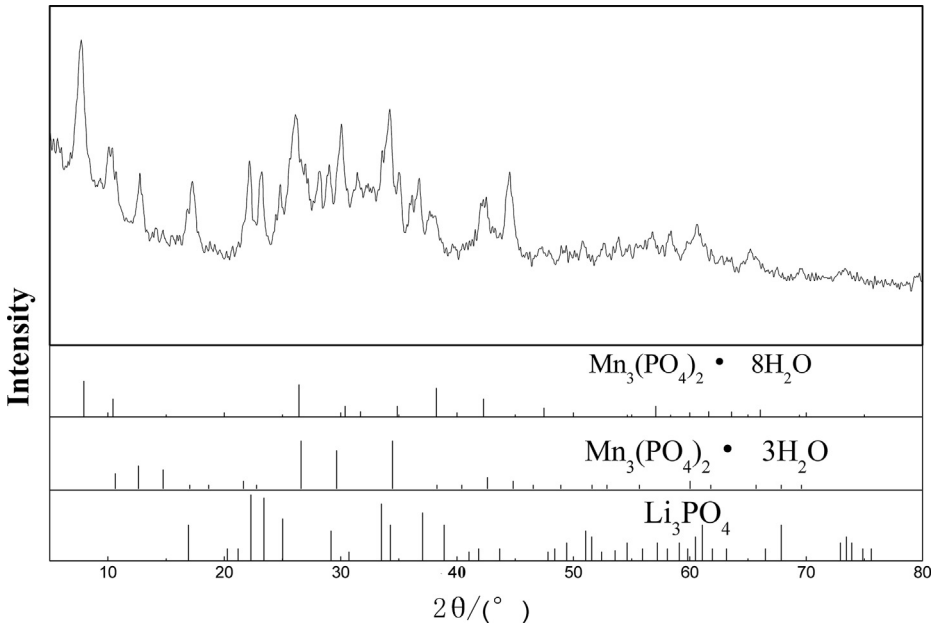

Fig. 2. The XRD pattern of the mixture slurry after 6 h mechanical activation treatment.

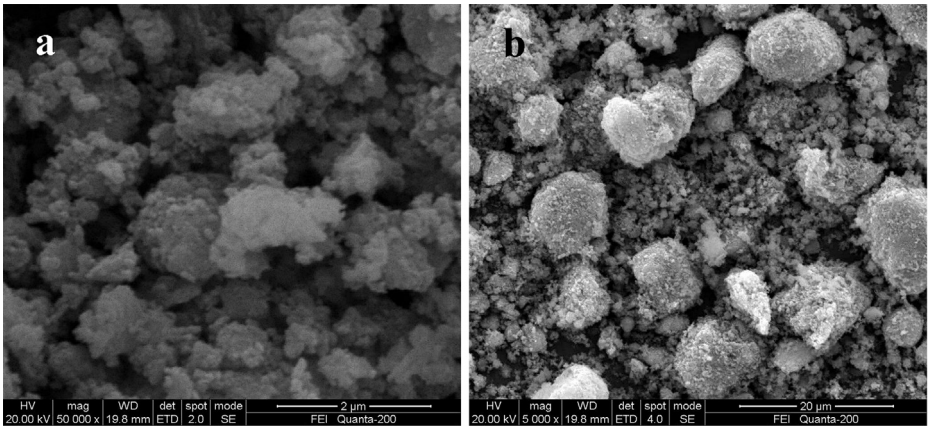

Fig. 3. The morphology of the as-prepared $Mn_3(PO_4)_2{\cdot}xH_2O + Li_3PO_4$ mixture after 6 h mechanical liquid activation reaction (a, ×50,000; b, ×5000).

X-ray diffraction (XRD) analysis was performed by X-ray diffractometer (XRD, D/max-r A type CuKα,40 kV, 300 mA, 10–80°). Scanning electronic microscopy (SEM JEOL JSM-6360LV) was performed to detect the surface morphology and analyze the size of the particles. The microstructure of the samples was examined by a Tecnai G12 transmission electron microscope (TEM). The mass of coated carbon was detected by infrared carbon sulfur analysis instrument (HW 2000).

The charge–discharge properties of $LiMnPO_4$ were investigated in CR2025 coin-type cells. A composite positive electrode was built by mixing the $LiMnPO_4$/C powders, a black carbon, and a PVDF binder in a weight ratio of 80:10:10. These were then coated onto an Al foil current collector and dried at 120 °C for 10 h in a vacuum oven. Circular discs with a diameter of 10 mm were punched out as the positive electrode. A disk of lithium foil was used as the negative electrode. As a separator we used a piece of Celgard 2400 membrane. 1 M $LiPF_6$/EC + DMC (50:50 vol%, Guotai, China) was applied as the electrolyte. The test cells were assembled in a glove box with an excellent environment control, the concentration of both H_2O and O_2 were below 1 ppm. The charge–discharge performance of the cells was conducted on a battery test system (Land CT 2001A, Land Co. China). The cells for rate tests were cycled between 2.5 V and 4.5 V vs. Li/Li^+ with CC–CV charging mode. Cells were charged at a constant current rate (0.05, 0.1, 0.2, 0.5, 1 or 2 C) to 4.5 V and kept at 4.5 V until the current rate decreased to C/50 ($1\ C = 170\ mA\ g^{-1}$), then discharged at a constant current rate (0.05, 0.1, 0.2 0.5, 1 or 2 C) to 2.5 V. In this report, coated carbon was considered as the active material in electrochemical performance test processes.

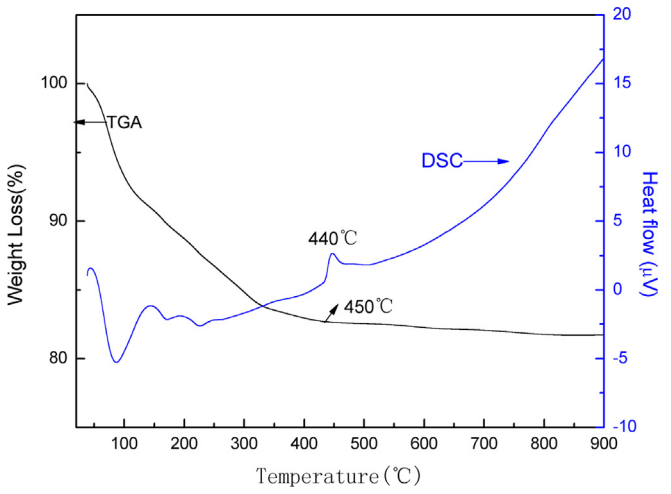

Fig. 4. TGA/DSC curves of precursor mixtures.

3. Results and discussion

Fig. 2 displays the XRD pattern of the mixture slurry after mechanical activation treatment for 6 h. It shows no evidence of diffraction peaks of Mn after 6 h mechanical liquid activation reaction. The structure of the mixture changes into $Mn_3(PO_4)_2{\cdot}xH_2O + Li_3PO_4$. However, the peaks intensity are low and wide. This process can be described by Reaction (1), in which only H_2 and H_2O are released from the first step as waste.

$$Mn + LiH_2PO_4 + 8/3H_2O \rightarrow 1/3Mn_3(PO_4)_2{\cdot}8H_2O + 1/3Li_3PO_4 + H_2\uparrow. \quad (1)$$

Fig.3 shows the morphology of the as-prepared $Mn_3(PO_4)_2{\cdot}xH_2O + Li_3PO_4$ mixture after 6 h mechanical liquid activation reaction. From the SEM images we can observe that the sample consists of secondary particles which are irregular in shape. These secondary particles are loosely aggregated, and the primary particles are also irregular in shape with uniform particle size distribution. Fortunately, the primary particle size is smaller than 100 nm. During the milling process, the powder particles undergo repeated welding, fracturing and rewelding in wet ball-milling, which results in pulverization, intimate powder mixing. Part of the mechanical energy transforms into enthalpy in the form of dislocation, defect, etc. stored in the milled powders. As the energy is continuously input into the milled powder the dislocation density increases with the continued milling. And then the solid–liquid reaction is induced to form new phosphate phases. Due to mechanical force, the newly formed phosphates precipitating on the surface of the Mn powder peels off and breaks into fine particles violently during the continuous collisions among the balls and between the balls with the wall of the cylinder. The fresh surface when the solid peeled off helps to accelerate the Mn dissolution reaction rate to form new reaction product layer. These cycles will not stop until the Mn powder is consumed. Meanwhile, ball milling can effectively arrest the undesirable crystal growth of phosphate phases ($Mn_3(PO_4)_2{\cdot}xH_2O + Li_3PO_4$). Combining the advantage of mechanical exfoliation in water-alcohol medial, a homogeneous precursor ($Mn_3(PO_4)_2{\cdot}xH_2O + Li_3PO_4$)/PVA with nanometer-sized particles can be obtained efficiently.

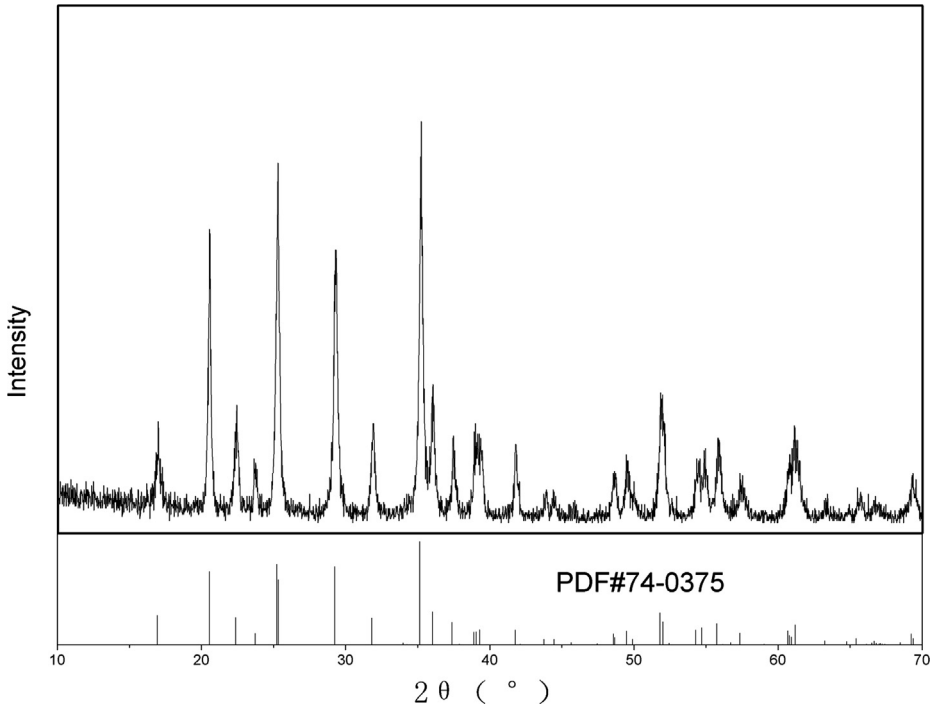

Fig. 5. The XRD patterns of $LiMnPO_4$/C synthesized at 650 °C.

The TGA/DSC curves of precursor mixtures are given in Fig.4. The thermogravimetric TG curve shows from 30 °C to 150 °C, corresponds to the loss of the surface water. A huge mass loss step lies from 150 to 350 °C, which can be assigned to the release of H_2O, CO_2, H_2 and hydrocarbons gas from the decomposition from the mixture of $Mn_3(PO_4)_2 \cdot xH_2O$ and PVA [30,31]. $LiMnPO_4$/C material forms below 350 ~ 450 °C with an obvious exothermic peak at 440 °C in the DSC curve. After 450 °C, the product weight decreases slightly, which may be caused by the pyrolysis of the remaining PVA. The TG/DSC curves also indicate that the formation of $LiMnPO_4$ and the conversion to amorphous carbon of PVA occur within the same temperature range. This suggests that it is possible to coat carbon simultaneously with the formation of $LiMnPO_4$ grain and restrict the growth of $LiMnPO_4$ particle during the heating treatment, resulting in synthesis of high-performance $LiMnPO_4$/C composite material. Fig.5 shows the XRD pattern of $LiMnPO_4$/C

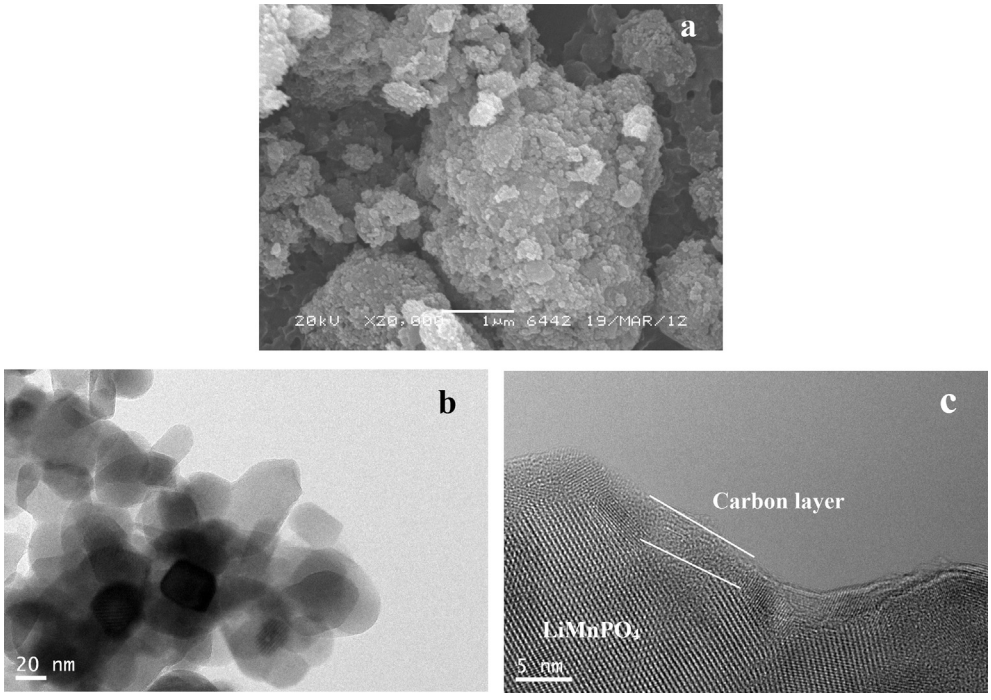

Fig. 6. The SEM (a) and TEM (b and c) images of $LiMnPO_4$/C samples calcined at 650 °C.

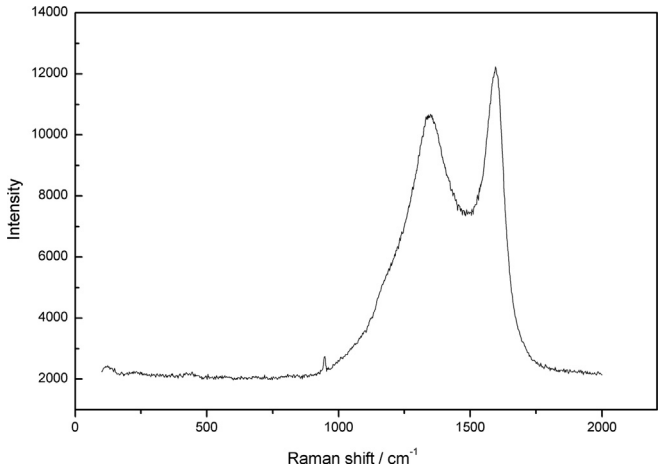

Fig. 7. Raman spectra of $LiMnPO_4/C$.

samples prepared at 650 °C, which fits well with the standard pattern of $LiMnPO_4$. The patterns match the standard XRD data for the $LiMnPO_4$ of PDF #74-0375, ICSD#25834, perfectly, indicating that the crystal structure of $LiMnPO_4$ is monoclinic systems with space group Pmnb (62). From the materials processing point of view, only H_2, CO_2 and H_2O are released from the whole synthesis process. It is considered economic, and eco-efficient.

The $LiMnPO_4/C$ particles calcined at 650 °C are examined by scanning electron microscopy (SEM) and transmission electron microscopy (TEM) to observe the morphology and nano structure of $LiMnPO_4$ grain. As shown in Fig. 6(a), the SEM images of $LiMnPO_4/C$ powders calcinated at 650 °C consist of particles with small size and uniform distribution, the primary particle size is smaller than 100 nm. TEM images of $LiMnPO_4/C$ particles are shown in Fig. 6(b), illustrating that the size of most $LiMnPO_4/C$ particles is in the range from 20 to 50 nm. The high resolution TEM image has shown in Fig.6(c) clearly reveals that primary particle is coated by continuous thin carbon film to form a $LiMnPO_4/C$, providing an intimate contact of carbon on $LiMnPO_4$ particles.

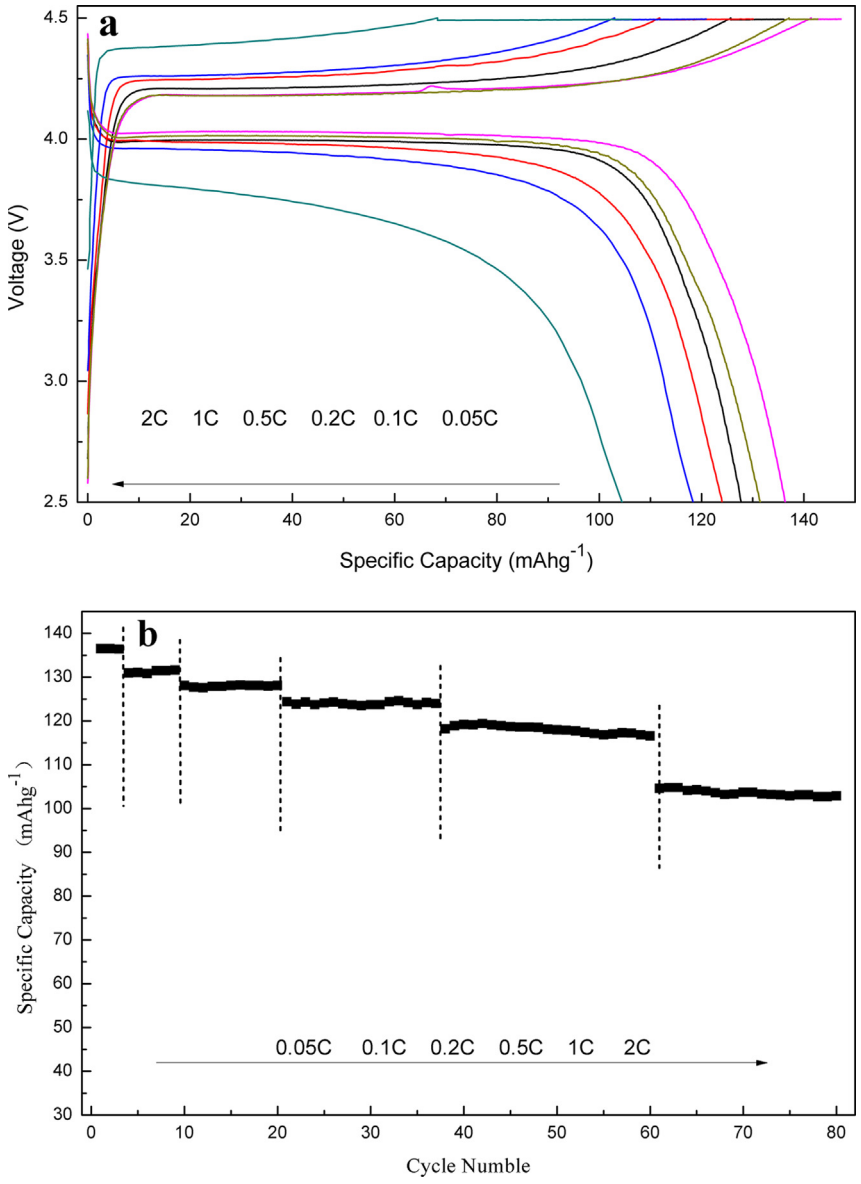

Fig. 8. The charge and discharge capacity curves (a) and discharge capacity vs. cycle number curve (b) for the $LiMnPO_4/C$ samples.

Lithium ions can easily intercalate into the conductive framework built through the in situ carbon conductive layer (thickness of about 2 nm).The carbon content in the products are prepared at 650 °C is 7.0 wt% according to carbon analysis result. In Raman spectra, showed in Fig.7, phosphate-related peak at 950 cm^{-1} turned clearly with two high intensity peaks assigned to carbon's D and G bands at 1345 cm^{-1} and 1590 cm^{-1}, which evidences the less carbon coating in our samples. Consequently, it indicates the residual pyorlyzed carbon of PVA in situ formed uniform conductive nano-film on the surface of $LiMnPO_4$ grain. It mainly benefits from the mechanochemical activation approach and a synchronous process between the decomposition into carbon of PVA and the phase formation of $LiMnPO_4$, which ensures the composite with ultrafine particle size and homogeneous carbon distribution.

To estimate the rate-capability of prepared $LiMnPO_4$/C active material, the cells were cycled between 2.5 and 4.5 V at 0.05, 0.1, 0.2, 0.5, 1 C and 2 C-rate. Fig. 8(a) shows the discharge curves of $LiMnPO_4$/C samples prepared at 650 °C. The $LiMnPO_4$/C exhibits good discharge capacity and excellent discharge plateaus. The capacity of the active samples at 0.05 C is 136.4 mAh g^{-1} and 118 mAh g^{-1} at 1 C-rate. As increasing the current density, the discharge capacity of $LiMnPO_4$/C decreases. The cycle performance of $LiMnPO_4$/C at various rates is displayed in Fig. 8(b). As has shown in the figure, the capacity retention is nearly 100% at various rates. The results indicate that as-prepared $LiMnPO_4$/C composites with reduced carbon amount exhibit good discharge capacity, discharge plateaus and stable cycle performance at various rates. It mainly attributes to the fine and uniform particle size and improved electronic conductivity through in situ carbon coating.

Fig. 9 shows the CV profiles of $LiMnPO_4$/C – Li cells after 1, 10 and 100 charge/discharge cycles under 0.2 C rate. The scanning rate is 0.1 mV s^{-1} from 2.5 to 4.8 V. There is only one peak pair, consisting of one anodic peak (charge) and one cathodic peak (discharge), which corresponds to the two-phase charge/discharge reaction of the Mn^{2+}/Mn^{3+} redox couple. From the CV curves for cells after 1 charge/discharge cycle and 10 charge/discharge cycles, the cathodic peak has a shift to the higher voltage and the anodic peak has a shift to the lower voltage, with higher peak intensity, suggesting the electrode reactivity is improved in the initial cycles. The reproducibility of the peaks in the CV plots confirms the good reversibility of lithium extraction/insertion reactions in the $LiMnPO_4$/C composites. Furthermore, both the CV curves and the insert discharge vs. cycle number curve show the good performance of our $LiMnPO_4$/C composite.

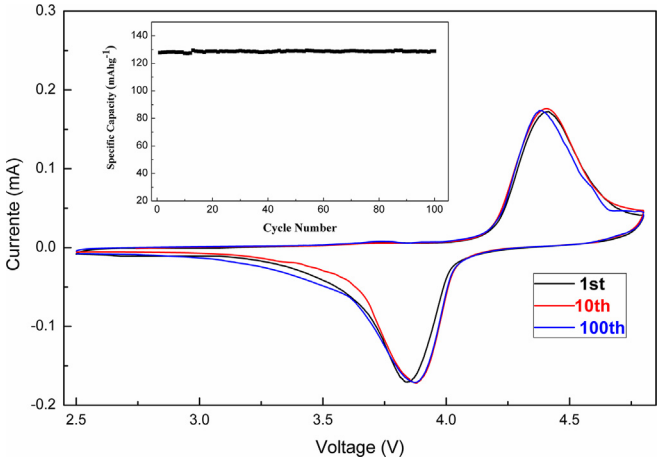

Fig. 9. The CV curves of $LiMnPO_4$/C – Li cells after 1, 10 and 100 charge/discharge cycles under 0.2 C rate at a 0.1 mV s^{-1} scanning rate from 2.5 to 4.8 V. Insert shows the cycle performance of $LiMnPO_4$/C under 0.2 C rate.

4. Conclusions

A novel efficient synthesis process was developed involving Mn and LiH_2PO_4 as raw materials and the addition of PVA as carbon source for syntheses $LiMnPO_4$/C nano compound material. By the new eco-efficient route, we achieved nano-sized ($Mn_3(PO_4)_2 \cdot xH_2O$ + Li_3PO_4)/PVA precursor successfully, which subsequently converted to 20 ~ 50 nm $LiMnPO_4$/C composites by a simple calcination step. The results indicate that as-prepared $LiMnPO_4$/C composites show well-ordered olivine-type structure, and exhibit good discharge capacity, excellent discharge plateaus and stable cycle performance at various rates. Consequently, it indicates that the mechano-chemical activation technique is very attracting for facile fabrication of $LiMnPO_4$/C in large scale.

Acknowledgment

The project was supported by the National Key Technology Research and Development Program of China (2007BAE12B01), Fundamental Research Funds for the Central Universities (2012QNZT018), China Postdoctoral Science Foundation (2012M521546).

References

[1] K. Zaghib, A. Guerfi, P. Hovington, A. Vijh, M. Trudeau, A. Mauger, J.B. Goodenough, C.M. Julien, J. Power Sources 232 (2013) 357–369.
[2] S.W. Lee, C. Carlton, M. Risch, Y. Surendranath, S. Chen, S. Furutsuki, A. Yamada, D.G. Nocera, Y. Shao-Horn, J. Am. Chem. Soc. 134 (2012) 16959–16962.
[3] A.K. Padhi, K.S. Nanjundaswamy, J.B. Goodenough, J. Electrochem. Soc. 144 (1997) 1188–1194.
[4] A. Yamada, M. Hosoya, S.C. Chung, Y. Kudo, K. Hinokuma, K.Y. Liu, Y. Nishi, J. Power Sources 119–121 (2003) 232–238.
[5] J. Xiao, N.A. Chernova, S. Upreti, X. Chen, Z. Li, Z. Deng, D. Choi, W. Xu, Z. Nie, G.L. Graff, J. Liu, M.S. Whittingham, J.G. Zhang, Phys. Chem. Chem. Phys. 13 (2011) 18099–18106.
[6] J. Su, B.Q. Wei, J.P. Rong, W.Y. Yin, Z.X. Ye, X.Q. Tian, L. Ren, M.H. Cao, C.W. Hu, J. Solid State Chem. 184 (2011) 2909–2919.
[7] T. Shiratsuchi, S. Okada, T. Doi, J.I. Yamaki, Electrochim. Acta 54 (2009) 3145–3151.
[8] N.P.W. Pieczonka, Z. Liu, A. Huq, J.H. Kim, J. Power Sources 230 (2013) 122–129.
[9] S.K. Martha, B. Markovsky, J. Grinblat, Y. Gofer, O. Haik, E. Zinigrad, D. Aurbach, T. Drezen, D. Wang, G. Deghenghi, I. Exnar, J. Electrochem. Soc. 156 (2009) A541–A552.
[10] D. Choi, D. Wang, I.T. Bae, J. Xiao, Z. Nie, W. Wang, V.V. Viswanathan, Y.J. Lee, J.G. Zhang, G.L. Graff, Z. Yang, J. Liu, Nano Lett. 10 (2010) 2799–2805.
[11] K. Su, F. Liu, J. Chen, J. Power Sources 232 (2013) 234–239.
[12] Y. Cao, J. Duan, G. Hu, F. Jiang, Z. Peng, K. Du, H. Guo, Electrochim. Acta 98 (2013) 183–189.
[13] K. Du, L.H. Zhang, Y.B. Cao, Z.D. Peng, G.R. Hu, Mater. Chem. Phys. 136 (2012) 925–929.
[14] J. Xiao, W. Xu, D. Choi, J.G. Zhang, J. Electrochem. Soc. 157 (2010) A142–A147.
[15] L. Wang, W. Sun, X. He, J. Li, C. Jiang, Int. J. Electrochem. Sci. 7 (2012) 3591–3600.
[16] D. Choi, J. Xiao, Y.J. Choi, J.S. Hardy, M. Vijayakumar, M.S. Bhuvaneswari, J. Liu, W. Xu, W. Wang, Z. Yang, G.L. Graff, J.G. Zhang, Energy Environ. Sci. 4 (2011) 4560–4566.
[17] K. Du, L.H. Zhang, Y.B. Cao, H.W. Guo, Z.D. Peng, G.R. Hu, J. Appl. Electrochem. 41 (2011) 1349–1355.
[18] C. Delacourt, C. Wurm, P. Reale, M. Morcrette, C. Masquelier, Solid State Ionics 173 (2004) 113–118.
[19] J. Zong, Q. Peng, J. Yu, X. Liu, J. Power Sources 228 (2013) 214–219.
[20] T.H. Kim, H.S. Park, M.H. Lee, S.Y. Lee, H.K. Song, J. Power Sources 210 (2012) 1–6.
[21] J. Chen, S. Wang, M.S. Whittingham, J. Power Sources 174 (2007) 442–448.
[22] J. Liu, X. Liu, T. Huang, A. Yu, J. Power Sources 229 (2013) 203–209.
[23] K. Dokko, T. Hachida, M. Watanabe, J. Electrochem. Soc. 158 (2011) A1275–A1281.
[24] X.L. Pan, C.Y. Xu, D. Hong, H.T. Fang, L. Zhen, Electrochim. Acta 87 (2013) 303–308.
[25] J. Ni, L. Gao, J. Power Sources 196 (2011) 6498–6501.

[26] S.L. Yang, R.G. Ma, M.J. Hu, L.J. Xi, Z.G. Lu, C.Y. Chung, J. Mater. Chem. 22 (2012) 25402–25408.
[27] S. Yang, M. Hu, L. Xi, R. Ma, Y. Dong, C.Y. Chung, ACS Appl. Mater. Interfaces 5 (2013) 8961–8967.
[28] P. Barpanda, K. Djellab, N. Recham, M. Armand, J.-M. Tarascon, J. Mater. Chem. 21 (2011) 10143–10152.
[29] D. Wang, H. Buqa, M. Crouzet, G. Deghenghi, T. Drezen, I. Exnar, N.H. Kwon, J.H. Miners, L. Poletto, M. Grätzel, J. Power Sources 189 (2009) 624–628.
[30] J.L. Shie, Y.H. Chen, C.Y. Chang, J.P. Lin, D.J. Lee, C.H. Wu, Energy Fuels 16 (2002) 109–111.
[31] Z. Peng, L.X. Kong, Polym. Degrad. Stab. 92 (2007) 1061–1068.